PROCEEDINGS, TOUGH Symposium 2006
Lawrence Berkeley National Laboratory, Berkeley, California, May 15–17, 2006

DEPRESSURIZATION-INDUCED GAS PRODUCTION FROM CLASS 1 AND CLASS 2 HYDRATE DEPOSITS

George J. Moridis, and Michael Kowalsky

Lawrence Berkeley National Laboratory
Berkeley, CA. 94702, USA
E-mail: GJMoridis@lbl.gov

ABSTRACT

Class 1 hydrate deposits are characterized by a Hydrate-Bearing Layer (HBL) underlain by a two-phase zone involving mobile gas. Such deposits are further divided to Class 1W (involving water and hydrate in the HBL) and Class 1G (involving gas and hydrate in the HBL). In Class 2 deposits, a mobile water zone underlies the hydrate zone. Methane is the main hydrate-forming gas in natural accumulations. Using TOUGH-FX/HYDRATE to study the depressurization-induced gas production from such deposits, we determine that large volumes of gas could be readily produced at high rates for long times using conventional technology. Dissociation in Class 1W deposits proceeds in distinct stages, but is continuous in Class 1G deposits. Hydrates are shown to contribute significantly to the production rate (up to 65% and 75% in Class 1W and 1G, respectively) and to the cumulative volume of produced gas (up to 45% and 54% in Class 1W and 1G, respectively). Large volumes of hydrate-originating CH_4 could be produced from Class 2 hydrates, but a relatively long lead time would be needed before gas production (which continuously increases over time) attains a substantial level. The permeability of the confining boundaries plays a significant role in gas production from Class 2 deposits. In general, long-term production is needed to realize the full potential of the very promising Class 1 and Class 2 hydrate deposits.

INTRODUCTION

Background

Gas hydrates are solid crystalline compounds in which gas molecules are lodged within the lattices of ice crystals. Under suitable conditions of low temperature and high pressure, a gas G will react with water to form hydrates according to

$$G + N_H H_2O = G \bullet N_H H_2O$$

where N_H is the hydration number. Of particular interest are hydrates formed by methane ($G = CH_4$), in which case $N_H = 6$. Natural gas hydrate deposits involve mainly CH_4, and occur in two distinctly different geologic settings: in the permafrost and in deep ocean sediments. Current estimates of CH_4 in hydrates vary widely, ranging between 10^{15} to 10^{18} m^3 (Sloan, 1998). Even the most conservative estimate surpasses by a factor of two the energy content of the total fossil fuel reserves recoverable by conventional methods. Even if a fraction is recoverable, the sheer magnitude of this resource demands technical and economic evaluation as a potential energy resource. Gas from hydrates can be produced by inducing dissociation by one of the following three main methods (Sloan, 1998): (1) depressurization, (2) thermal stimulation, and (3) the use of hydration inhibitors (e.g., salts and alcohols).

Classification of hydrate deposits. Natural hydrate accumulations are divided into three main classes (Moridis and Collett, 2003; 2004). Class 1 accumulations are composed of two layers: an underlying two-phase fluid zone with free (mobile) gas, and an overlying the hydrate interval involving water and hydrate (Class 1W) or gas and hydrate (Class 1G). In Class 1 deposits, the bottom of the hydrate stability zone (i.e., the location above which hydrates are stable because of thermodynamically favorable P and T conditions) coincides with the bottom of the hydrate interval. This class appears to be the most promising target for gas production because the thermodynamic proximity to the hydration equilibrium requires only small changes in P and T to induce dissociation (Moridis and Collett, 2003). Additionally, the existence of a free gas zone guarantees gas production even when the hydrate contribution is small. Class 2 deposits comprise two zones: (1) a hydrate-bearing interval, overlying (2) a mobile water zone. In Class 2 deposits, the entire hydrate interval may be at or well within the hydrate stability zone.

Objective. The main objective of this study is to evaluate the production potential of Class 1 and Class 2 accumulations by means of depressurization, and to determine the factors and conditions affecting it. Depressurization appears to be an attractive method because of its simplicity, technical and economic effectiveness, and the fast response of hydrates to the rapidly propagating pressure wave.

The Numerical Model

The numerical studies were conducted using the TOUGH-Fx/HYDRATE code (Moridis et al., 2005a), which can simulate the non-isothermal hydration reaction, phase behavior and flow of fluids and heat in natural CH_4-hydrate deposits involving complex geologic media. It includes both an equilibrium and a kinetic model (Kim et al., 1987) of hydrate dissociation. The model accounts for heat and up to four mass

components (i.e., water, CH_4, hydrate, and water-soluble inhibitors such as salts or alcohols) that are partitioned among four possible phases: gas, aqueous, ice, and hydrate. A total of 12 states (phase combinations) can be described by the code (of which 9 are shown in Figure 1), which can handle any combination of hydrate dissociation mechanisms.

PRODUCTION FROM A CLASS 1W DEPOSIT

Case 1: Description

The geometry and properties of the system in this case are shown in Figure 2 and are listed in Table 1. The hydraulic and thermal properties of the porous media were the same in the hydrate and in the free-gas zones. The reservoir radius was R_{max} = 567.5 m. The initial P and T distributions followed the hydrostatic and geothermal gradients, respectively. The impermeable (but heat-exchanging) upper and lower bounding formations were each 30 m thick. Gas was produced through a single well at the center of the reservoir. To prevent hydrate formation near the wellbore, the z = -30 m to -57 m interval of the wellbore (with z = 0 set at the top of the upper boundary) was heated at a rate of 500 W/m. The producing interval was from –46 m to –56 m, i.e., 1 m below the initial hydrate interface, thus preventing steep pressure P and temperature T gradients that could lead to secondary hydrate formation and "choke" the well. In the hydrate zone, the initial hydrate and aqueous phase saturations (S_H and S_A, respectively) were consistent with levels encountered in permafrost deposits (Dallimore et al., 1999).

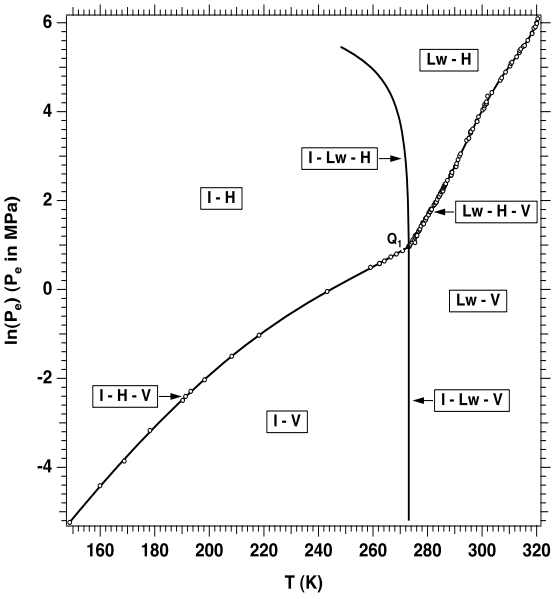

Figure 1. P-T equilibrium relationship in the phase diagram of the H_2O–CH_4–hydrate system (Moridis et al., 2005a).

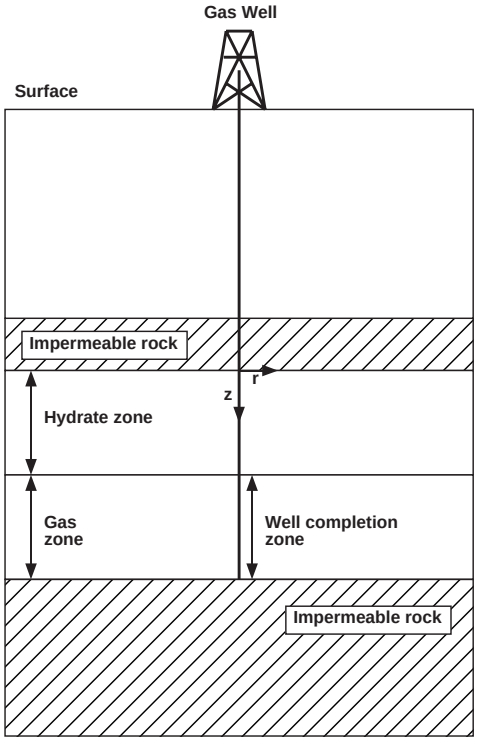

Figure 2 – Depressurization-induced production from a Class 1 hydrate deposit in Case 1.

Grid and Simulation Specifics

The system was simulated using a 2-D cylindrical grid. The domain was discretized in 90 x 94 = 8,460 gridblocks in (r,z), of which 8,280 were active and the remaining were boundary cells. The top and bottom grid layers were constant-temperature, no-flow boundaries, while the grid layers corresponding to the 30-m-thick top and bottom confining layers were impermeable but allowed heat exchange with the deposit. In the radial direction, the Δr series followed a logarithmic distribution. The HBL was subdivided uniformly along the z-direction into 60 segments of Δz = 0.25 m each. In the free-gas zone, Δz ranged between 0.25 m and 1 m. This discretization provided a high level of detail near the wellbore and in the entire HBL. Using the equilibrium hydration reaction option in TOUGH-FX/HYDRATE (Moridis et al., 2005a), the grid resulted in 24,840 coupled equations.

Results and Discussion of the Class 1W Study

To describe gas production from Class 1 hydrates, we employ the concepts of *Rate Replenishment Ratio* (RRR) and *Volume Replenishment Ratio* (VRR) that were proposed by Moridis et al. (2005b). RRR is the fraction of the gas production rate Q_P that is replenished by CH_4 released from hydrate dissociation. VRR is the fraction of the cumulative produced CH_4 volume (V_P)

Table 1. Conditions and Properties in Case 1

Parameter	Value
Gas zone thickness	15 m
Hydrate zone thickness	15 m
Initial P (at interface)	1.067×10^7 Pa
Initial T (at interface)	286.65 K
Gas composition	100% CH_4
Permeability $k_r=k_z$	10^{-12} m^2 (= 1 D)
Porosity ϕ	0.30
Initial aqueous and gas saturations (free gas zone)	S_A, S_G from capillary pressure
Initial hydrate and aqueous saturations (hydrate zone)	$S_H = 0.7$, $S_A = 0.3$
Initial gas production rate	0.82 ST m^3/s (= 2.5 MMSCFD)
Dry thermal conductivity	0.5 W/m/K
Wet thermal conductivity	3.1 W/m/K
Capillary pressure model (Moridis et al., 2005b)	Equation (7)
c	-0.65
P_e	1.55×10^4 pa
w	9.28
a	2.1
b	2.2
Relative permeability model (Stone, 1970) and Original Porosity Model (Moridis et al., 2005b)	$k_{rA} = (S_A^*)^n$ $k_{rG} = (S_G^*)^n$ $S_A^*=(S_A-S_{irA})/(1-S_{irA})$ $S_G^*=(S_G-S_{irG})/(1-S_{irA})$
n	3
Irreducible gas saturation S_{irG}	0.02
Irreducible aqueous Phase saturation S_{irA}	0.25

that has been replenished by CH_4 from hydrates. These two parameters provide a measure of the hydrate system response and the effectiveness of depressurization-induced dissociation as a gas-producing method. The evolution of the volumetric rate of CH_4 release from the hydrate (Q_R) and of the corresponding Q_P are shown in Figure 3(a). Review of Figure 3 and study of the corresponding simulation results lead us to identify four stages – marked in Figure 3(b) – during gas production from Class 1W deposits. These are discussed below.

Stage I. Stage I corresponds to dissociation from two main zones: the initial horizontal hydrate interface and a cylindrical interface around the well. A second horizontal hydrate interface evolves at the top of the hydrate interval and then advances downward. The reason for the emergence of the second horizontal interface is a combination of depressurization with heat exchange with the overburden. An additional phenomenon observed in Phase I is the beginning of evolution of a *hydrate channeling* system, i.e., a system of narrow conductive channels alternating with impermeable high-S_H bands that advance into the body of the hydrate in a 'wormhole-like" manner aligned with the general direction of flow.

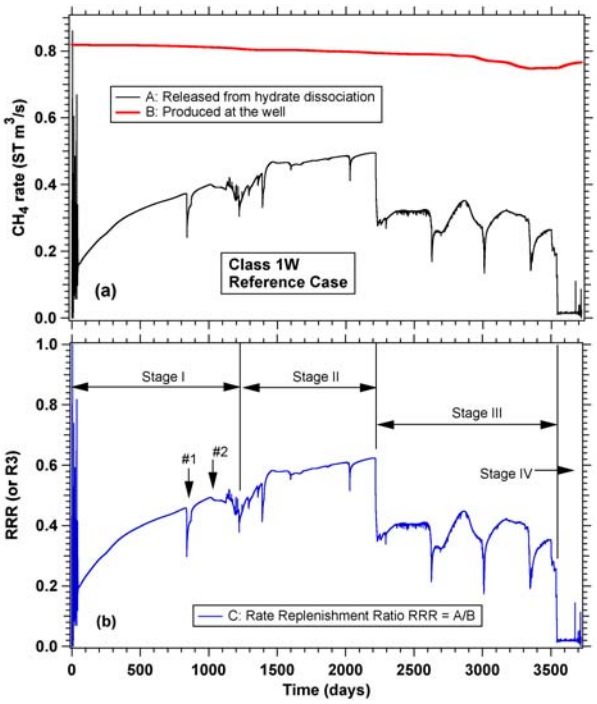

Figure 3. Evolution of Q_R (A), Q_P (B), and the corresponding RRR (C) during long term production from a Class 1W hydrate deposit.

The hydrate channels are a consequence of the hydrate lensing process (caused by capillary pressure) described by Moridis et al. (2005b), with the alternating high-low S_H bands formed along the direction of fluid flow. These provide access to the interior of the hydrate body and an additional diffuse dissociation surface. Hydrate channels are dynamic features, in which the high-S_H bands can continue to expand at the expense of the aperture available for flow. The end of Stage I is marked by the drop in RRR in Figure 3b, which occurs when the effects of hydrate channeling and lensing begin to have a significant effect on flow and hydrate dissociation. At the end of Stage I, the cylindrical dissociation zone is roughly uniform and extends to the upper boundary. Point #1 in Figure 3b indicates exhaustion of the lowermost grid layer of hydrate, and point #2 marks the dissociation front reaching the upper boundary.

Stage II. In Stage II, dissociation continues along the two horizontal interfaces (upper and lower) and the cylindrical interface. This stage is characterized by full development of the hydrate channels, which represent an additional dissociation zone. After its decline at the end of Phase I, RRR begins to increase because of the increased pressure drop brought about by the evolution of the hydrate channels. Hydrate lensing continues during Stage II, the end of which is marked by a precipitous drop in RRR. This is caused by the "sealing" of the entire bottom (horizontal) boundary by an impermeable hydrate lens character-

ized by a very high S_H, in which S_A and S_G fall below their irreducible levels. Employing the conservative approach described by Moridis et al. (2005b), the simulation results provide the lower limit of the gas production estimate, with a large fraction of the high-S_H hydrate mass being treated as inert.

Stage III. In Phase III, only the cylindrical and the upper horizontal interfaces are active dissociation fronts. The dissociation zone created by the hydrate channels is also active, but hydrate lensing (Moridis et al., 2005b) continues to accumulate hydrates, increasing S_H and decreasing the aperture of the "wormholes". In this stage, the hydrate channels play a critical role in providing hydraulic communication between the upper hydrate interface, the overlying hydrate-free layer, and the interior of the hydrate zone. Compared to Stages I and II, RRR is lower in Stage III and has a downward trend because (a) the total area of dissociation is reduced by the very large bottom horizontal boundary (now occluded), (b) the remaining dissociating regions are more distant from the well, and (c) are connected to the hydrate-free zone mainly through the limited cross-sectional area of the progressively less conductive hydrate channels.

Stage IV. The onset of Stage IV is marked by another precipitous drop in the RRR value to levels below 0.1. This indicates a dramatic reduction in dissociation activity and is caused by (a) occlusion of the upper interface by a hydrate shell, or (b) through closure of the hydrate channels (Moridis et al., 2005b). At this stage, dissociation occurs in only a few isolated gridblocks either on the vertical wall of the cylindrical interface or served by still-open channels within the main hydrate body.

General observations. In Figure 3 we observe that (a) Q_R attains high levels early, and (b) it increases with time in Stage I and II. Thus, after less than 3 months of production, over 25% of the production rate is replenished from hydrate dissociation. At the end of Phase II (at about 6.2 years), dissociation proceeds at a rate of 0.533 ST m^3/s and replenishes about 65% of the production rate. Even with the decline in dissociation in Stage III, RRR averages about 40%. Comparison of the cumulative volume of CH_4 released from dissociation (V_R) to V_P leads to the VRR shown in Figure 4, which confirms the early contribution of hydrates to gas production in addition to the hydrate potential as a very productive gas source. VRR continues to increase rapidly through Stages I and II, with 47% of V_P at the end of Stage II having been replenished from hydrate dissociation. Because of decreasing dissociation, VRR declines during Stage III and more rapidly in Stage IV. At the end of the 10-year production period, the VRR value indicates that about 42% of the total gas volume produced up to that point (i.e., 1.08×10^8 ST m^3) has been replenished from dissociation.

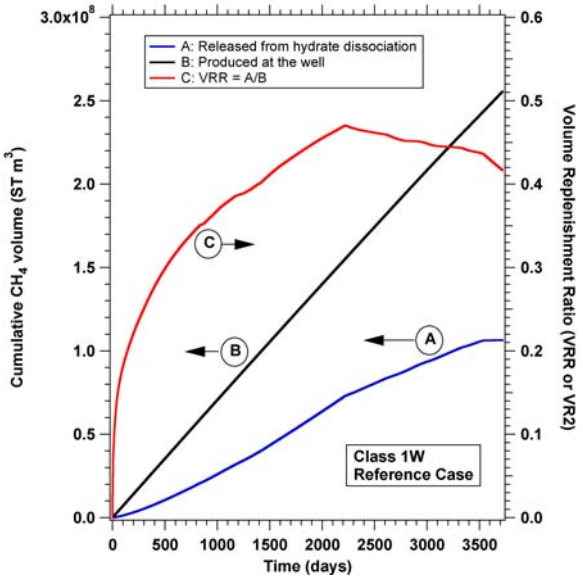

Figure 4. Evolution of V_R (A), V_P (B) and the corresponding VRR (C) during production from the Class 1W deposit in Figure 3.

The corresponding water production is limited over the 10-year production period (Figure 5). These results indicate the technical feasibility and the effectiveness of using dissociation to readily produce large amounts of gas at high rates using conventional technology. Note that the depressurization process described in this paper does not have any technical requirements that cannot be addressed with current state-of-the-industry capabilities.

Evolution of Hydrate Distribution. Some of the most interesting observations can be made from the distribution of S_H in Figure 6. Figure 6b reveals the expansion of the cylindrical interface radially from the wellbore during Stage I. The upper interface becomes evident after t = 4 years, i.e., at the beginning of Stage II (Figure 6c). The most striking feature in Figure 6 is the emergence of the banded S_H distribution of the hydrate channels, which becomes more pronounced with time as they advance into the hydrate body. The hydrate channels are evident at t = 4 years. These "wormhole-like" structures appear to permeate a large portion of the main hydrate body during Stage III (t = 6 years, Figure 8e) and an even larger one in Stage IV (Figure 6f, t = 10 years). An interesting feature of the hydrate channels is that they are roughly aligned with the flow lines to the well.

Along with the hydrate channels, hydrate lenses evolve at the lower horizontal hydrate interface, which continues to dissociate and to move upward until the end of Stage III. The alternating high-low S_H bands are evident at t = 4 years (Figure 6c), and continue to expand until the end of Stage III, after which time they no longer change.

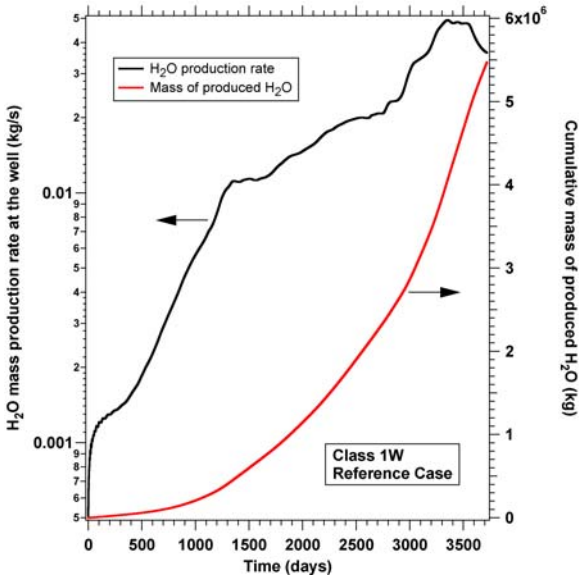

Figure 5. Water production during gas production from the Class 1W deposit in Figures 3 and 4.

In Stage IV, dissociation has ceased in the bulk of the hydrate body because of occlusion, and only proceeds in isolated subregions mainly on the cylindrical hydrate interface. One such pocket with the appearance of an intrusion into the hydrate body is evident in Figure 6f. The drastic decline in hydrate dissociation in Stage IV is due to reductions in (a) the extent of the active dissociation regions, in (b) their permeability and in (c) their cross-sectional area available to flow.

PRODUCTION FROM A CLASS 1G DEPOSIT

Case 2: Description

The system configuration, geometry, and properties in this case are very similar to those in the Class 1W case, from which it differs in the following:

(1) The intrinsic permeability $k = 4.325 \times 10^{-14}$ m^2.
(2) In the HBL, $S_H = 0.7$ and $S_G = 0.3$.
(3) The rate of wellbore heating to prevent hydrate formation was 200 W/m of wellbore.
(4) The capillary pressure is now given by the van Genuchten model (1980) as,

$$P_{cap} = -P_0 \left[\left(S^* \right)^{-1/\lambda} - 1 \right]^{\lambda}, \quad S^* = \frac{(S_A - S_{irA})}{(S_{mxA} - S_{irA})} \quad \text{..... (1)}$$

with $S_{mxA} = 1$, $\lambda = 0.6$, and $P_0 = 1890$ Pa.

Results and Discussion of the Class 1G Study

The (a) volumetric rate of depressurization-induced CH_4 release from the hydrate, (b) the production rate at the well, and (c) the corresponding RRR over the 30-year simulation period appear in Figure 7 and exhibit a drastically different pattern from that in Case 1. The RRR in Figure 7 does not show any sign of the distinct stages identified in Class 1W deposits (Figure 4), and seems to indicate that dissociation from hydrates in Class 1G deposits is a continuous process. This is attributed to the high gas mobility in the hydrate zone. The steep, short-duration drops in the CH_4 release rate and the RRR are related to discretization effects, and occur when dissociation is complete along a given layer. The exhaustion of the hydrate removes a source of gas (in addition to causing a T drop in adjacent layers) and results in the temporary drop in the release rate. Figure 7 also shows that the hydrate contribution to production increases monotonically with time. At the end of the 30-year production period, an impressive 75% of the rate of gas production has been replenished by CH_4 from hydrates. Compared to the Class 1W case, RRR increases significantly slower in Class 1G deposits because of the much larger gas volume, in addition to the much larger gas compressibility. These observations lead to the conclusion that long-term production is needed to realize the full potential of the very promising Class 1G hydrate deposits.

Comparison of V_R and V_P leads to the VRR shown in Figure 8. VRR rises rapidly early, increases continuously with time, and shows that 54% of the produced volume at the end of the 30-year production period has been replenished from hydrate dissociation. By that time, 4.13×10^8 ST m^3 have been released from dissociation in this relatively small deposit. These results further confirm the technical feasibility and the effectiveness of using dissociation to readily produce large amounts of gas at high rates using conventional technology. The attractiveness of Class 1G deposits is further enhanced because water production remains very low during the entire 30-year production span, as shown in Figure 9.

PRODUCTION FROM A CLASS 2 DEPOSIT

Case 3: Description

The geometry of Case 3 is described in Figure 1. Table 2 lists the system properties and initial conditions that are different from those in Case 1. The reservoir radius was R_{max} = 908 m. As in the previous two cases, the impermeable but heat-exchanging layers above the hydrate zone and below the water zone were each 30 m thick. Reservoir fluids were produced through a single well at the center of the reservoir at a constant rate of 9.48 kg/s (5000 BPD). The producing interval was located in the top 5 m below the initial hydrate interface.

Grid and Simulation Specifics

The system consisted of five single-well sections. Each section was simulated using a 2-D cylindrical grid. The domain was discretized in 40 x 31 = 1,240 gridblocks in (r,z), of which 1,160 were active and the remaining were boundary cells.

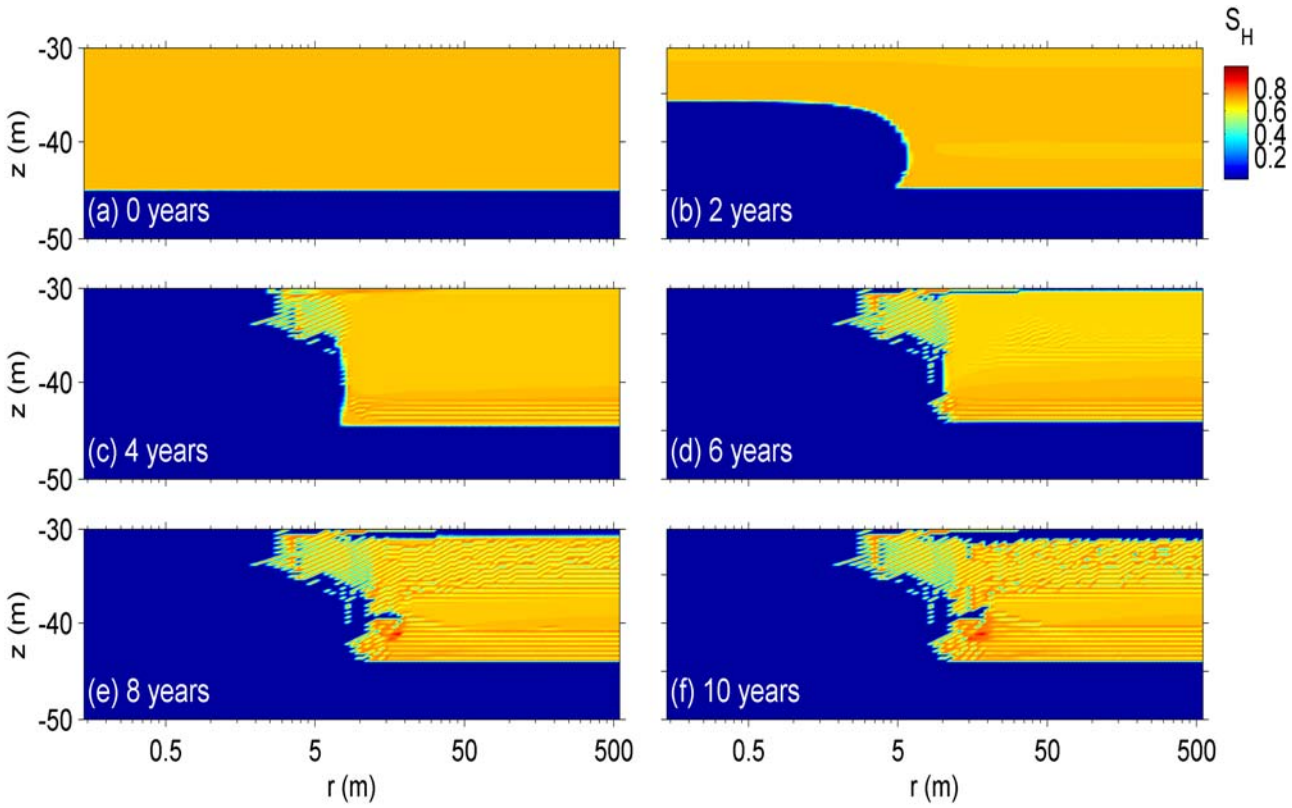

Figure 6 – Evolution of the hydrate saturation distribution during depressurization-induced gas production from a Class 1W hydrate deposit.

The tip and bottom grid layers in the discretized domain corresponded to no-flow, constant-temperature boundaries that followed the standard geothermal gradient dT/dz = 0.03 °C/m. The 30-m-thick top and bottom confining layers were impermeable but allowed heat exchange with the deposit. Compared to the grid in the case of the Class 1W and 1G deposits, the grid in the Class 2 study was coarser in both the r and the z directions. The initial P and T distributions in the system were determined from the hydraulic and geothermal gradients in relation to the reference P and T at the hydrate interface (see Table 2). Using the equilibrium hydration reaction option in TOUGH-Fx/HYDRATE (Moridis et al., 2005a) and accounting for the effects of salinity, the grid resulted in 4,640 coupled equations. Note that the results we report in the Class 2 study correspond to the cumulative performance of the five single-well sections.

Results and Discussion of the Class 2 Study

Figure 9 shows the evolution of (a) the rate Q_R of CH_4 release from hydrate dissociation into the reservoir, and (b) the rate Q_P of CH_4 production at the well. In Class 2 hydrate deposits, $Q_R > Q_P$ because of the need for gas to accumulate until S_G exceeds the irreducible S_{irG} before flowing to the well. Obviously, desirable representatives of Class 2 deposits should be characterized by large and converging Q_R and Q_P. Figure 10 shows that this is indeed the case. Because of the very low compressibility of water, the depressurization effect is immediate, leads to the release of large volumes of CH_4, and Q_R increases monotonically during the 8.56 years of production.

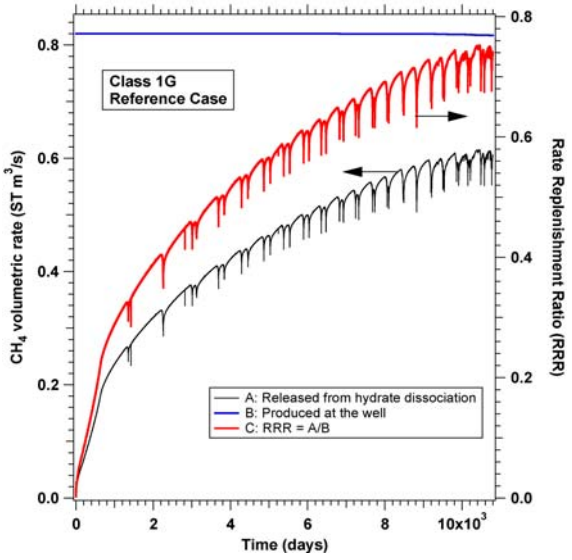

Figure 7. Evolution of Q_R (A), Q_P (B), and the corresponding RRR (C) during long term production from a Class 1G hydrate deposit.

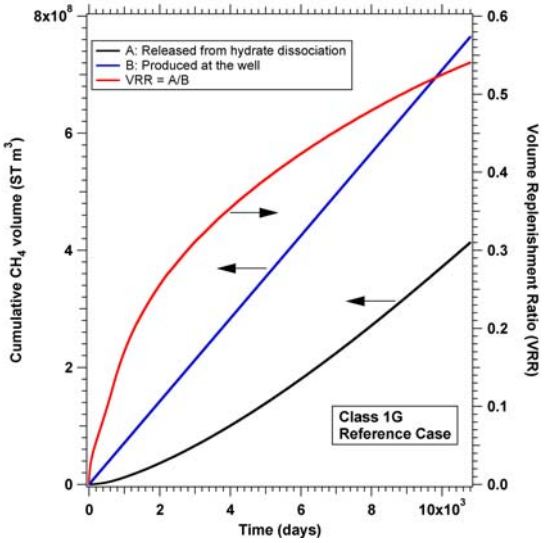

Figure 8. Evolution of V_R (A), V_P (B) and the corresponding VRR (C) during production from the Class 1G deposit in Figure 7.

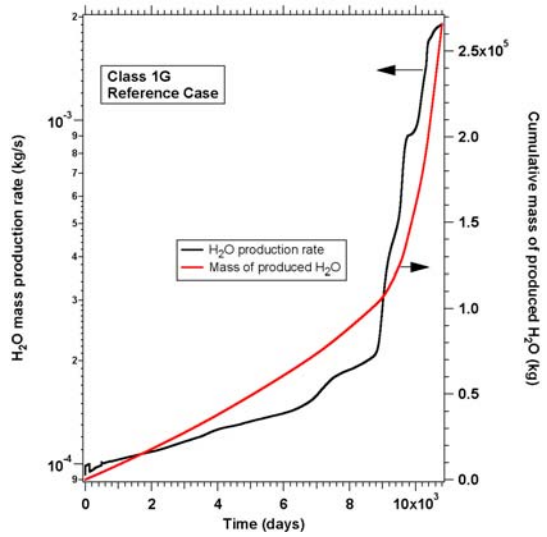

Figure 9. Water production during gas production from the Class 1G deposit in Figures 7 and 8.

Although it takes over a year before a substantial CH_4 production is observed at the well, Q_P continues to increase and to converge toward Q_R during the study period. At t = 8.56 years, Q_P reaches the very attractive level of 1.19×10^6 ST m^3/day (i.e., about 2.38×10^5 ST m^3/day per well), which represents about 74% of Q_R. This very large volume of produced gas indicates the attractiveness of Class 2 deposits as potential energy sources. The S_G distribution in Figure 11 shows the presence of a sizeable gas bank (all of which emanating from hydrate dissociation) centered about the hydrate interface. This free gas zone extends along the entire reservoir radius, penetrates 2 m into the water zone, and extends about 6 m into the hydrate zone.

Table 2. Conditions and Properties in Case 3

Parameter	Value
Water zone thickness	10 m
Hydrate zone thickness	50 m
Initial P (at interface)	1.024×10^7 Pa
Initial T (at interface)	284.45 K
Porosity ϕ	0.38
Initial hydrate and aqueous saturations (hydrate zone)	$S_H = 0.7$, $S_A = 0.3$
n in relative permeability model (Stone, 1970)	3.567
Irreducible aqueous phase saturation S_{irA}	0.20

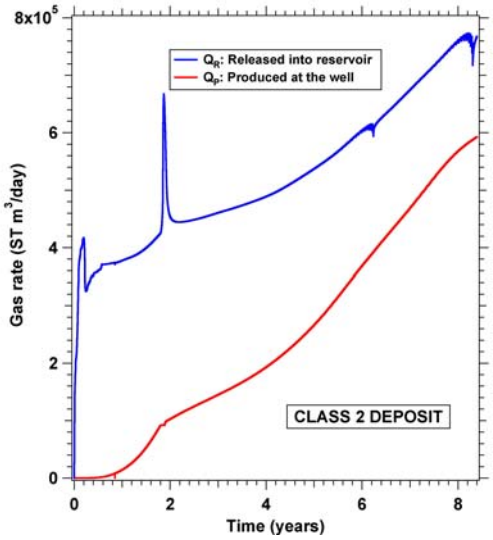

Figure 10. Evolution of Q_R and Q_P during production from a Class 2 hydrate deposit.

Case 4: Effect of Boundaries in Production From a Class 2 Deposit

Figure 12 shows the effect of boundaries on gas production from Class 2 deposits. This case differs from Case 3 in that (a) the upper boundary is now permeable (with k = 10^{-14} m^2 and ϕ = 0.38), (b) the water zone is 300 m thick, and (c) the fluid withdrawal rate is 38.6 kg/s (20,000 BPD). Figure 12 shows the evolution of Q_R and Q_P over time. The Q_R pattern is marked by an initial steep increase, followed by a decline and eventual stabilization. Figure 12 indicates that (a) Q_P represents a small fraction of Q_R, (b) Q_P is very low (about 100 ST m^3/day), stabilizes early and does not improve over with time, and (c) is accompanied by a prohibitive water production rate of about 3,150 m^3/day. This disappointing performance is attributed to the reduced effectiveness of depressurization in the presence of permeable boundaries and deep-water zones, and indicates that simple depressurization is not a promising production method from this kind of Class 2 deposits.

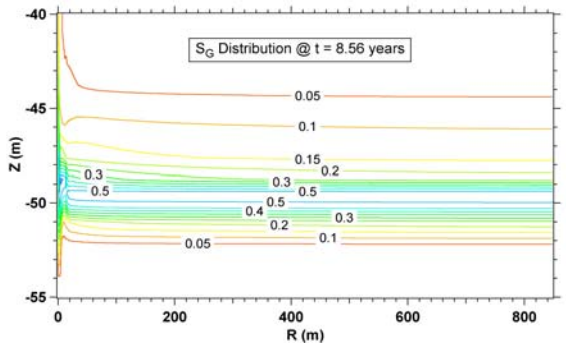

Figure 11. Distribution of gas saturation S_G in the Class 2 deposit of Case 3 at t = 8.56 years.

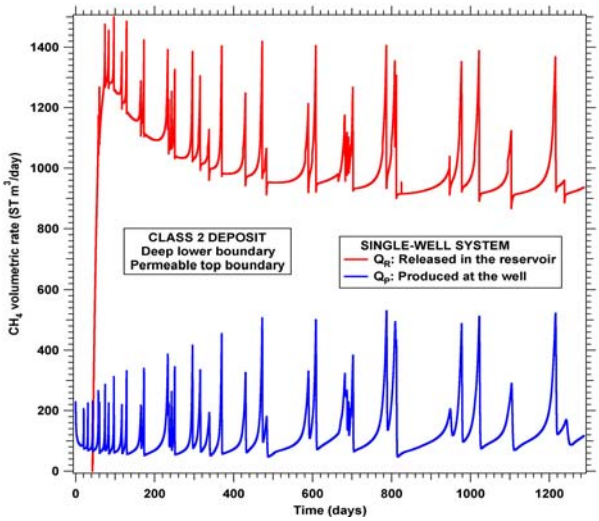

Figure 12. Evolution of Q_R and Q_P during production from the Class 2 hydrate deposit in Case 4.

SUMMARY AND CONCLUSIONS

1. Large volumes of gas can be readily produced at high rates for long times from Class 1 gas hydrate accumulations, by means of depressurization-induced dissociation using conventional technology.
2. There are up to four stages of system response in Class 1W hydrates under production. Stages I and II are associated with expanding dissociation interfaces and the formation of hydrate lenses and channels within the HBL. Stages III and IV are associated with partial and complete occlusion, respectively, of the hydrate. Gas release from dissociation attains high levels early, increases with time in Stages I and II, declines in Stage III, and drastically so in Stage IV.
3. In Class 1W deposits, up to 65% of the production rate and 45% of the produced volume are replenished with gas from hydrate dissociation.
4. Production from Class 1G deposits is continuous, free of the stages identified in Class 1W deposits, and increases monotonically with time. Up to 75% of the rate of gas production is replenished by gas releases from hydrate dissociation.
5. Water production remains very low during the production from Class 1 hydrate deposits.
6. Large gas volumes can be recovered from Class 2 deposits if water disposal does not pose a problem. Although large volumes of gas are released into the reservoir early during depressurization, substantial production begins after a relatively long lead time.
7. In Class 2 deposits, (a) the rate of release into the reservoir Q_R exceeds the production rate Q_P, but (b) they both increase monotonically with time and (c) follow a converging evolution pattern.
8. Simple depressurization is an ineffective gas production method from Class 2 deposits with permeable boundaries and deep water zones.
9. The full benefits of depressurization-induced dissociation in Class 1 and Class 2 accumulations are realized in long-term production regimes.

ACKNOWLEDGEMENTS

This work was supported by the Assistant Secretary for Fossil Energy, Office of Natural Gas and Petroleum Technology, through the National Energy Technology Laboratory, under the U.S. Department of Energy, Contract No. DE-AC03-76SF00098. The authors thank Matt Reagan, John Apps and Dan Hawkes for their thorough review.

REFERENCES

Dallimore, S.R., Uchida, T., and Collett, T.S. (eds.), Scientific Results from JAPEX/JNOC/GSC Mallik 2L-38 Gas Hydrate Research Well, Mackenzie Delta, Northwest Territories, Canada, Geological Survey of Canada Bulletin 544, 1999.

Kim, H.C., Bishnoi, P.R., Heidemann, R.A., and Rizvi, S.S.H., Kinetics of methane hydrate decomposition, *Chem. Eng. Sci*., 42(7): 1645-1654, 1987.

Moridis, G.J., and Collett, T.S., *Strategies for Gas Production From Hydrate Accumulations Under Various Geologic Conditions*, LBNL-52568, Lawrence Berkeley National Lab., Berkeley, CA, 2003.

Moridis, G.J., Kowalsky, M.B., and K. Pruess, *TOUGH-Fx/HYDRATE v1.0 User's Manual: A Code for the Simulation of System Behavior in Hydrate-Bearing Geologic Media*, Report LBNL-58950, Lawrence Berkeley National Lab., Berkeley, CA, 2005a.

Moridis, G.J., Kowalsky, M.B., and Pruess, K., *Depressurization-Induced Gas Production From Class 1 Hydrate Deposits*, SPE 97266, 2005 SPE Annual Technical Conference and Exhibition, Dallas, Texas, U.S.A., 9 – 12 October 2005b.

Sloan, E.D., *Clathrate Hydrates of Natural Gases*, Marcel Dekker, Inc., New York, NY, 1998.

Stone, H.L., Probability model for estimating three-phase relative permeability, *Trans. SPE of AIME*., 249: 214-220, 1970.

van Genuchten, M. Th., A closed-form equation for predicting the hydraulic conductivity of unsaturated soils, *Soil Sci. Soc. Am. J*., 44: 892-898, 1980.